The Application of Advanced Methods in Analyzing the Performance of the Air Curtain in a Refrigerated Display Case — Source link ↗

Homayun K. Navaz, Ramin Faramarzi, Morteza Gharib, Dana Dabiri ...+1 more authors

Institutions: Kettering University, Edison International, California Institute of Technology

Related papers:

- Jet entrainment rate in air curtain of open refrigerated display cases

- CFD simulation of refrigerated display cabinets

- The use of CFD to improve the performance of a chilled multi-deck retail display cabinet

- Simulation of the performance of single jet air curtains for vertical refrigerated display cabinets

- Two- and three-dimensional CFD applied to vertical display cabinets simulation

Homayun K. Navaz
Associate Professor of Mechanical Engineering,
Kettering University,
Flint, MI 48504

Ramin Faramarzi
Refrigeration and Thermal Test Center
Project Manager,
Southern California Edison Company,
Irwindale, CA 91702

Morteza Gharib
Professor of Aeronautics,
California Institute of Technology,
Pasadena, CA 91125

Dana Dabiri
Research Scientist,
California Institute of Technology,
Pasadena, CA 91125

Darius Modarress
President,
Viosense Corporation,
Pasadena, CA 91106

The Application of Advanced Methods in Analyzing the Performance of the Air Curtain in a Refrigerated Display Case

Computational Fluid Dynamics (CFD) modeling is effectively coupled with the experimental technique of Digital Particle Image Velocimetry (DPIV), to study the flowfield characteristics and performance of the air curtain of a medium-temperature open vertical refrigerated display case used in supermarkets. A global comparison of the flowfield and quantification of the entrained air into the case indicate that there is a considerable amount of cold air spillage from a typical display case that is replaced by the ambient warm entrained air across the air curtain, lowering the energy efficiency of the case. The computational model that is developed from the marriage of CFD and DPIV techniques provides a reliable simulation tool that can be used for the design optimization of air curtains. A correct estimate of the infiltration rate by changing different parameters in a validated computational simulation model will provide a feasible tool for minimizing the spillage of the cold air, and thereby designing more energy efficient open display cases.
[DOI: 10.1115/1.1478586]

Introduction

Refrigerated display cases are extensively used in supermarkets and grocery stores. Recirculated cold air is used to keep the case contents at a desired preset temperature, while allowing customers unhindered access to the refrigerated food. Cold air is supplied into the case at the top through a discharge grill, and is recirculated through a return air grill at the bottom. Figures 1(*a*) and 1(*b*), show schematics of the display case with discharge and return air grills, and corresponding dimensions. The primary function of the cold air stream is to create a barrier between the outside warm air and the inside cold air. The effectiveness of the air curtain may depend on several factors including: the discharge air angle of throw, discharge air velocity (DAV), discharge air grill width, dimensional characteristics of the honey comb located at the discharge air grill, display case geometry, return air system, discharge air temperature (DAT), and number of air bands.

Laboratory tests have shown that infiltration constitutes the largest cooling load component of an open vertical display case [1]. So far, there has been no comprehensive qualitative and quantitative study of the flowfield parameters and structure for display cases. Stribling et al. [2] have made an attempt to combine the CFD and experimental results to study the velocity and turbulence in a display case. Their research indicates some discrepancies between the experimental and computational results, and they attribute that to the order of the numerical scheme and the grid resolution. Their hybrid approach of combining the computational and experimental methods to tackle the display case problem is genuine, but it is not conclusive. They have also recommended further research in this area.

One of the important aspects of such hybrid studies must be geared towards the optimized design of display cases, i.e., minimizing the infiltration of the outside air or better performance of the air curtain, and therefore energy savings. A cost effective optimization process requires a numerical simulation tool such as CFD methodology. On the other hand, reasonable confidence in

CFD results must be built through validation with "good" experimental data, therefore necessitating a combined, or a hybrid, study. The CFD technology can be utilized with a reasonable degree of confidence only if it is properly anchored on actual and accurate data.

Earlier experimental studies by the Southern California Edison (SCE) Company recognized the importance of optimized design of display cases and its significant impact on energy savings. These studies prompted SCE to sponsor further research in the area of display case flowfield modeling. Therefore, a joint effort by SCE, California Institute of Technology (CalTech), and Kettering University was initiated. SCE established the base case scenarios by conducting tests at its sophisticated Refrigeration and Thermal Test Center (RTTC). CalTech conducted the DPIV effort, and Kettering University was mainly responsible for the CFD modeling. The Digital Particle Image Velocimetry experimental technique was utilized for flow visualization, quantitative measurements of the velocity profile, and entrainment calculations. The ROYA$^{©}$ [3] computer code was the simulation tool for the CFD modeling. In this paper, we intend to address the importance of the problem and its potential impact on energy savings, validate the CFD code with experimental data in a global manner, and utilize the numerical simulation to estimate the infiltration rate as a function of two operating variables: the inlet air velocity, and temperature. This parametric study can be utilized to develop compact equations for the infiltration rate as a function of the inlet air velocity and temperature. Such equations are quite important and useful to manufacturers in the design of their cooling systems. Furthermore, this work will pave the road for minimization of the infiltration rate, i.e., optimization of the vertical display case design.

Initial Tests

The control environment and data acquisition system of SCE's RTTC was utilized to establish the foundation of the project. The controlled environment room is an isolated thermal zone served by independent cooling, heating and humidification systems. This allows simulation of various indoor conditions of a supermarket. The sensible cooling load representing people and other heat gain sources is provided by a constant volume direct expansion system

Transactions of the ASME
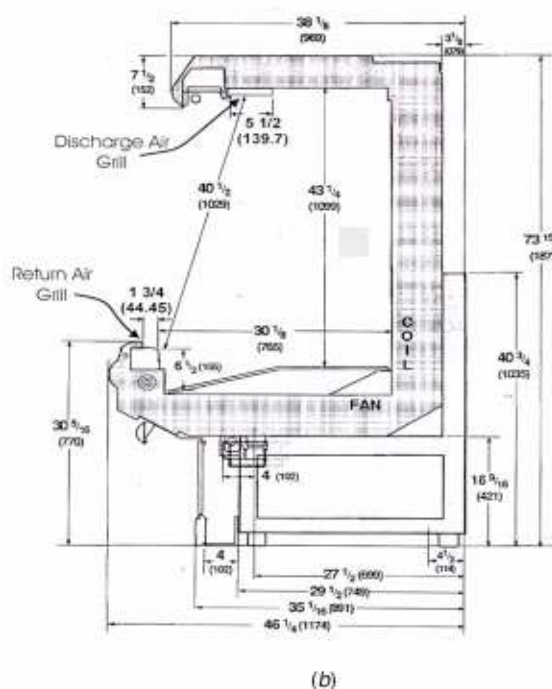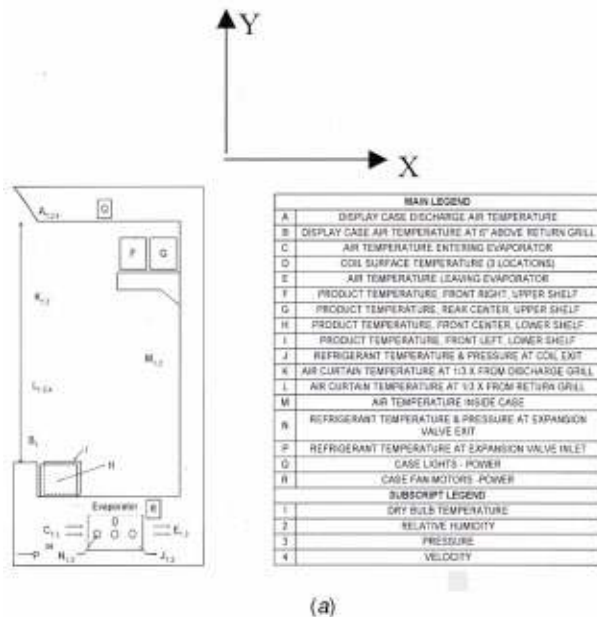
Fig. 1 (a) Case schematics and sensor locations with discharge and return grills. (b) Schematic of the display case with dimensions. (c) Simulator and dummy products used in the display case. (d) Multi-deck display case used in the present study.

reclaiming the waste refrigeration heat via a six-row coil. Auxiliary electric heaters located in the down-stream of the heat reclaim coils provide additional heating when required. While the air is conditioned to a desired thermostatic set point, an advanced ultrasonic humidification unit introduces precise amounts of moisture to the air surrounding the display case, representing the latent load due to outside air and people.

Discharge air velocity and temperature were selected as an ini-

tial set of test variables to ascertain the order of infiltration dependency on momentum and/or energy components of airflow. A series of initial tests were conducted to develop critical temperature and velocity readings within the display case. The fan blade pitch of the evaporator was changed from 34° to 11° to develop two discharge air velocity readings. Additionally, the refrigeration system suction pressure was changed from 53 psig (365.37 kPa gage) to 49 psig (337.80 kPa gage), resulting in 29.09°F

Table 1 Parameters used for each scenario

Test Scenario	Fan blade pitch	Measured average temperature °F (°C)	Reynolds number at $\frac{1}{2}$ of air curtain
1	34° (DAV* = 0.68 ms^{-1})	27.63 (−2.43)	26,766.
2	34° (DAV* = 0.68 ms^{-1})	29.09 (−1.62)	26,030.
3	11° (DAV* = 0.57 ms^{-1})	27.63 (−2.43)	23,144.

*Measured at discharge air grill.

(−1.62°C) and 27.63°F (−2.43°C) discharge air temperature, respectively, while DAV remained at 133 ft-min^{-1}, or 0.68 ms^{-1}. All modifications took place while the indoor condition of the room was maintained at 70°F (21.1°C) dry bulb (DB) and 45% relative humidity (RH).

All tests were conducted under American Society of Heating and Air-Conditioning Engineers (ASHRAE) Standard 72-1983, which prescribes a uniform method of testing of open refrigerators for food stores. This standard dictates that the air movement must be parallel to the plane of the opening of the display case and there should not be any external air drafts blowing into the refrigerated display case. The lighting intensity of the controlled environment room should be no less than 75 foot-candles (22.86 m-candle) at the center of the test fixture opening at a distance of one foot from the air curtain. This standard further dictates that the display case shall be filled with test package (or product simulator) and dummy products to simulate the presence of food product in the cases. According to ASHRAE Standard 72- 1983, food products are composed of 80 to 90 percent water, fibrous materials, and salt. A plastic container completely filled with a sponge material that is soaked in a brine solution of water and salt (6% by mass) was used to simulate the product. Figure 1(c) shows the simulator and dummy products.

Table 1 shows the parameters used for each test. In Test Scenarios 1 and 2, the fan speed is the same, i.e., the velocity of the inlet air remains constant while its average discharge air temperature varies. The comparison of these two test scenarios along with the results of parametric studies will be used to determine the temperature dependency of the volumetric flow rate of infiltrating air. In Test Scenario 3, the average temperature of the discharge air is maintained at the same value as the Test Scenario 1. However, with a smaller fan blade pitch, the average discharge air velocity was reduced. The comparison of these two tests will be used to determine the velocity dependency of the entering air.

Experimental Method

Digital Particle Image Velocimetry (DPIV) is a technique that is capable of measuring fluid velocity within a two-dimensional domain, unlike the hotwire or Laser Doppler Velocimetry (LDV) probe measurements that are single point measurement techniques. The present experiment was performed using FlowVision, a state-of-the-art DPIV system provided by General Pixels.

An Nd:Yag laser is used in combination with sheet generating optics to illuminate the cross-section of the flow of interest. The flow is then seeded with reflective particles that are small enough to accurately follow the flow. Upon illumination, the particles within the laser sheet reflect laser light. A camera situated at 90 degrees from the incident laser sheet captures the images within the laser sheet. These sequential images are recorded and post-processed, as explained below, to obtain the velocity and streamline fields.

The FlowVision implementation of the DPIV method is the cross-correlation technique, implying that sequential pairs are processed to produce a velocity field. For each sequential pair, a small interrogation window sub-samples a portion of each of the images at the same locations and a cross-correlation is performed, resulting in the average shift of particles within the interrogation windows. This interrogation is then, through calibration, con-
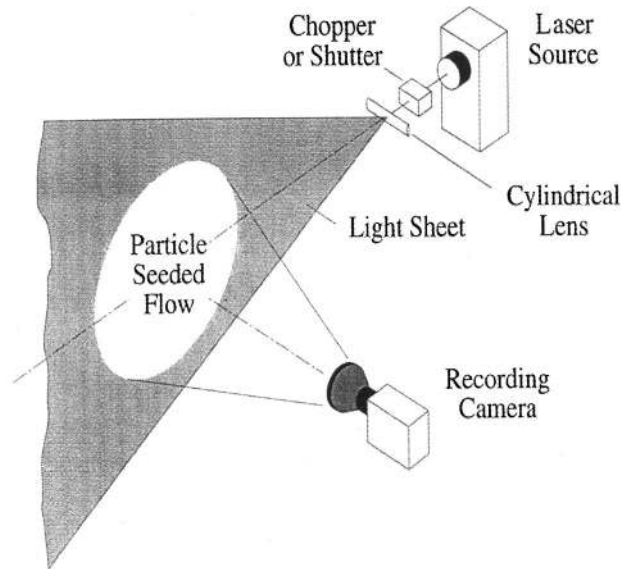
Fig. 2 Typical DPIV experimental setup

verted into a velocity vector. The interrogation window is systematically moved through the sequential images to produce a vector field. Once the vector field is obtained through time, they are averaged to produce the mean velocity flows and streamlines. More detailed information about the DPIV technique can be found in Willert and Gharib [4], Westerweel, Dabiri and Gharib [5], and Gharib and Dabiri [6].

For the present experiment, a 768*480 pixel camera acquired images at 30 frames per second. A 120-mJ Nd:Yag laser is used to create a laser sheet and illuminate the area of interest. As the work is done in air, smoke is used to generate finely particulated flow. A cross-section of the middle of a typical multi-deck display case is illuminated (see Figs. 1(d) and 2), roughly spanning an area of 40 by 40 inches (1.01×1.01 meters). The measurements were done near the mid-section of the case and away from the end plates to avoid any corner effects. In order to properly and accurately image the jet curtain emanating from the top of the display case, the whole flow regime was broken down into 20 separate and overlapping regions, each of which was interrogated with FlowVision. For each of the 20 sections, 1000 images were acquired, and their results were averaged. The images were interrogated using a 32 by 32 pixel window, with a 50% overlap ratio resulting in 1440 vectors per region. A typical experimental setup using FlowVision is shown in Fig. 2. The resolution of the PIV velocity measurements is 1% of the measured velocity. This number reflects the magnitude of the error in the experimental data.

Computational Method

In general, computational fluid dynamics (CFD) is a methodology by which the conservation, or Navier-Stokes (NS), equations are solved. The method primarily consists of approximating the exact partial derivatives by a finite change of a variable in time
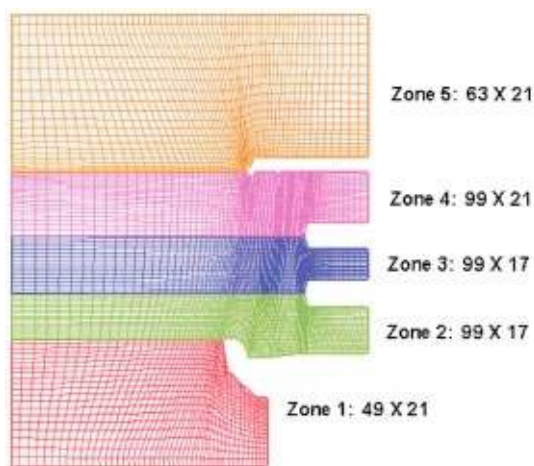
Fig. 3 Computational grid and zones

Labels within figure:
Zone 5: 63 X 21
Zone 4: 99 X 21
Zone 3: 99 X 17
Zone 2: 99 X 17
Zone 1: 49 X 21

and/or space. Although CFD provides a powerful tool for simulation of a problem, it is still an approximation and requires validation with experimental data.

The ROYA$^{©}$ computer program has been the simulation tool for this research. This code is a Navier-Stokes (NS) solver for compressible and incompressible flows with chemical reaction capabilities based on a structured grid. The earlier version of this code, called Liquid Thrust Chamber Performance (LTCP), was developed for the National Aeronautics and Space Administration (NASA) in the early to mid-90's [7] for dense spray combustion in liquid rocket engines. However, the algorithm is quite versatile, and the code has been exercised over a wide range of flow regimes from creeping to subsonic and supersonic flows with and without chemistry, for a wide range of applications [8, 9]. The discretization scheme is fully implicit, and the left (L) and right (R) states of the inviscid fluxes are based on the Total Variation Diminishing (TVD) method. Either the Lax-Friedrichs (LF) or the Van-Leer (VL) method can be implemented to calculate the total inviscid fluxes by combining the left and right states. Two turbulence models, Cebeci-Smith algebraic, and low Reynolds number k-ε, are embedded in the code. The solver is second order accurate in time and space. However, the spatial accuracy can be increased to fourth order. The method becomes first order in space across a shock due to the implementation of the flux limiter.

The display case is enclosed in a room (test area). The computational domain is composed of the entire room and the display case. The upper and lower boundaries are assumed to be no-slip adiabatic walls. The left boundary (see Fig. 3) is mainly a no-slip adiabatic wall except the lower part that is open to the atmosphere with a specified backpressure. The entire domain is decomposed into five zones as seen from Fig. 3. In the numerical simulation model, there is not any recirculating air through the ductwork. There is a constant supply of air through the discharge grill at measured velocities i.e., both components of velocity profiles across the grill are specified as taken by measurements (U and V). The measurements are taken in the middle of the display case to be compatible with the two-dimensional CFD analysis. The discharged air temperature is also measured and specified as a boundary condition for the CFD code. Due to the elliptic nature of the equations, it is evident that the density has to be specified using the information taken from the interior nodes and cannot be prescribed at the boundary. A backpressure that produces a mass flow rate equal to the integrated input flow rate from the supply grill, and back panel is selected by running the CFD code several times. This is a subsonic outflow, and only one flow variable, in this case pressure, can be specified. The rest of the information (U, V, and T) has to be taken from the interior nodes. Since the net mass flow rate into the case should be zero, any spillage can

directly be related to the entrained air. There is a supply of cold air through a perforated back panel with a very small inlet velocity (see Fig. 1(d)). In the simulation model, the amount of this cold air supply is uniformly distributed throughout the back panel. Since the mass balance is of the primary interest of this work, the net inflow of mass into the display case could not be compromised in the calculations. However, the uniform distribution of mass over the back panel will somewhat affect the temperature distribution in the display case and will cause a minor shift in the position of the cold air curtain as it will be seen from the results.

The amount of mass supplied from the discharge air grill and perforated back panel must be equal to the mass leaving the domain from the return air grill. Therefore, the amount of air leaving the display case by spillage can be marked by a negative axial velocity component (U), and the amount of air entering the display case can be marked by a positive axial component of velocity. The integrated mass flow across the negative U stencil represents the amount of spillage. This quantity is equal to the amount of mass flow rate across the positive U stencil. Calculation of the infiltration rate via the DPIV method verifies our numerical simulation method.

In the present analysis the Chien k-ε turbulence model for low Reynolds number is used. To carry the model to the wall a high-resolution grid is needed that causes a significant increase in the computational time. To avoid this problem, the two-equation k-ε model is used for the core flow and is linked to Cebeci-Smith algebraic model near the wall region. Although this method requires more programming skills, it is generally more advantageous over the law-of-the-wall approach. The edge of the sub layer where the algebraic and k-ε models are coupled can be determined by the Baldwin-Lomax vorticity, or total enthalpy criteria. These methods are described in [10, 11].

In the simulation model, the turbulence production term (k) was assumed to be 7.5% of the square of the average total velocity, i.e., $k = 0.075\bar{V}^2$. Turbulent dissipation was taken from the one equation model, i.e., $\varepsilon = C_D k^{2/3}/\ell$, where ℓ is the mixing length taken from the previous time step ($\ell = \nu_T/\sqrt{k}$), and C_D is the closure coefficient taken to be 0.08. These boundary conditions will reproduce the same turbulence intensity as measured data at the discharge air grill.

Verification and Validation of Results

Two components of the inlet air jet velocity profile near the discharge grill are shown in Fig. 4. At the discharge grill, the velocity is not uniform. For a perfectly symmetrical and undisturbed flow, the maximum vertical velocity occurs at the center and changes to zero at the wall. However, due to the subsonic nature of the flowfield, i.e., the elliptic characteristic of the NS
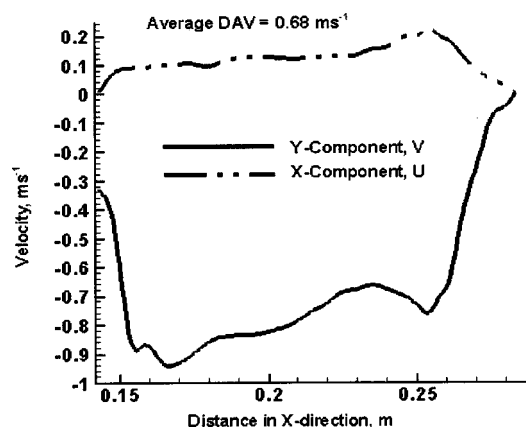

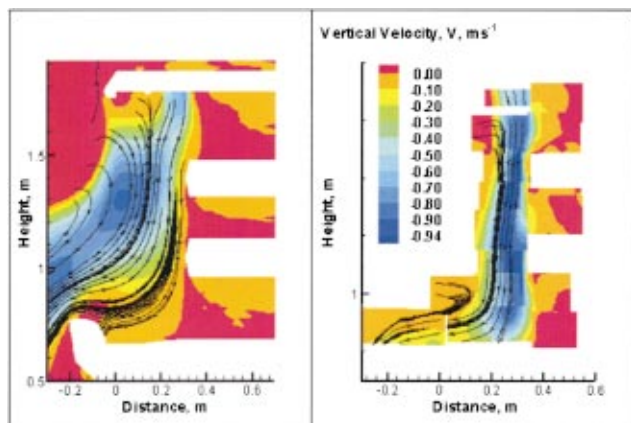**Fig. 4 Air velocity profile at the display case outlet for Scenario 1**

Fig. 5 Mean velocity and streamline fields for Scenario 1

Fig. 6 Axial velocity contours at the opening

equations, this ideal profile will be disturbed. Furthermore, the cold air discharge velocity profile depends on the movement of air throughout the entire domain, that is, the display case and ambient air. The horizontal component is seen to be positive, indicating that the flow is moving towards the display case at the edge of the grill. This may be a result of the design of the discharge grill geometry. The velocity boundary conditions for the CFD analysis were taken from this measurement. In CFD modeling, the products in the display case were also included and they were treated as a no-slip adiabatic wall. Although the surface temperature of the products can be measured and used as a boundary condition in the CFD code, it was decided to adopt a simple adiabatic wall condition due to small effects of temperature on the infiltration rate.

Figure 5 compares the predicted and observed vertical velocity contours and streamlines. Note that the velocity scales are identical for computational and experimental results. Streamlines obtained by CFD and experimental results reveal the nature of the interaction of the two-dimensional jet flow with the surrounding area. The streamlines emanating from the jet at the top of the display case are turned into the display case. This jet then flows downward across the edges of the upper shelves, and onto the lower shelf. When the jet reaches the lower shelf, it turns toward the left and outside of the display case. The vertical velocity contours show that the flow between the shelves is rather stagnant and hardly moves as compared with the air curtain. Therefore, it is postulated that it may take some time before steady-state temperatures are reached between the shelves once the refrigeration system is turned on. Streamline and velocity plots in Fig. 5 show that, for the most part, the jet is rather effective in creating an air curtain. However, this curtain does spill over at the lower part of the display case near the return air grill. This provokes an entrainment from ambient air. The spillage to the outside of the case is a source of discomfort to people in the vicinity. There is not a straightforward way to quantify the amount of the entrained ambient air.

As can be seen from Fig. 5, the entrained air is entering into the display case through a mixing process. This mixing mechanism for air contributes to the amount of the entrained ambient air. Figure 6 is a contour plot of the axial component of the velocity, and will provide the key to this calculation. Basically the entrained air replaces the amount of air that is spilled over from the display case. It is clear that the x-component of the velocity, U going toward the left, i.e., the negative x-direction, is the sole contributor to the spillage phenomenon in the numerical simulation as it was described earlier. Therefore, a line that originates from the bottom edge of the opening and extends to a location where $U = 0$ before it becomes positive, i.e., spans over all negative values of U, represents the surface that the air is moving
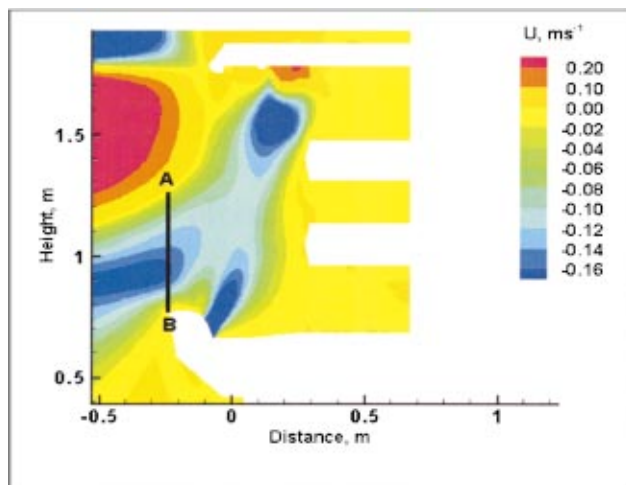
through and resulting in spillage. The AB line in Fig. 6 marks the negative U stencil. Therefore, integrating the velocity over this area will yield the volumetric flow rate of the spilled air that is equivalent to the entrained ambient air or the infiltration rate.

As was mentioned earlier, it is quite important to predict the amount of warm air that flows into the display case due to the overspill of the cold air. This infiltration rate is most likely a function of velocity for a given geometry and design. The continuity equation determines the amount of mass that is being transported from one location to another. For a fixed geometry, the characteristic length or area remains constant. On the other hand, due to the relatively incompressible nature of the flow, small temperature changes of the supplied cold air, and the fixed ambient air temperature, the density variation has a second order effect on the mass flow rate. Therefore, velocity emerges as the main flowfield parameter that controls the mass flow rate, that is, the infiltration of the ambient air into the display case. Furthermore a quantitative comparison between CFD and DPIV results for both components of velocity along the opening of the display case becomes indispensable. Figure 7 compares components of velocity that are extracted from the field data along a line that connects the bottom part of the display case near the return air grill to the discharge air grill. In Fig. 7, the data is extracted from Fig. 5 via the Tecplot©
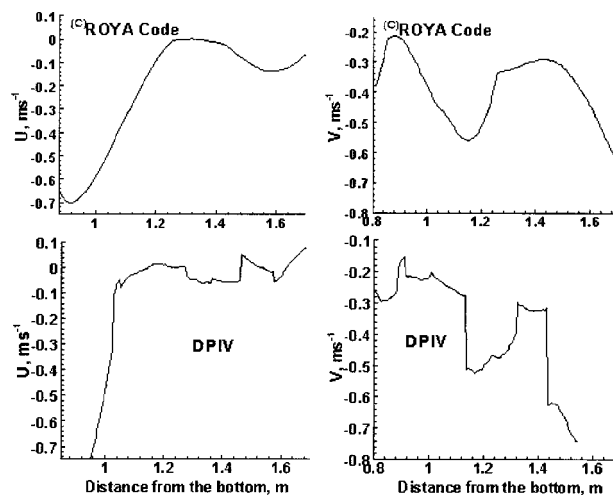

Fig. 7 Components of velocity profile along the display case opening as predicted by the CFD and DPIV techniques for Scenario 1
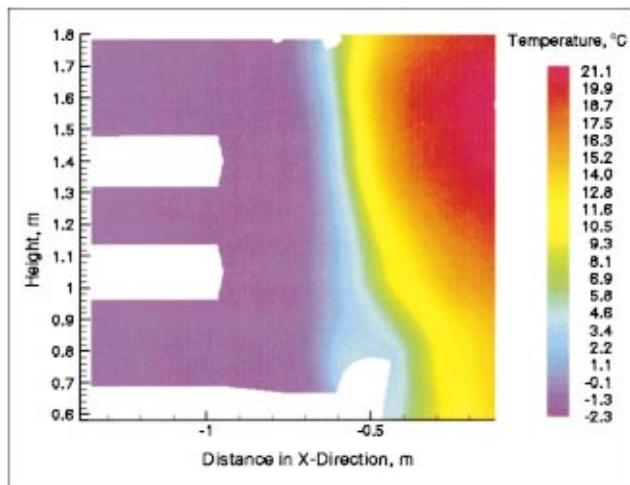
Fig. 8 CFD results for temperature contours in Scenario 1

quantity increases to 0.178 ms^{-1} in the shear layer and in the vicinity of edges. This quantity corresponds to a turbulence intensity of about 20%.

Figure 8 shows the temperature distribution predicted by the CFD model. The surroundings or far-field temperature is assumed to be 70°F (21.1°C). The space above the upper shelf is maintained as the coldest spot in the entire display case. This can be attributed to the positive component of axial velocity at the discharge grill as is seen in Fig. 4. Furthermore, Fig. 5 reveals somewhat stagnant air over the shelves contributing to fairly uniform cold temperature after achieving steady-state operation. However, this pattern breaks down toward the bottom shelf, due to a relative increase in mixing length and consequently the turbulence intensity. The onset of the break down of the jet emanating from the discharge grill is a function of the jet velocity, and also the structure of the mixing region that contributes to the infiltration of the outside air. That is, as the vortex that is mainly responsible for the mixing becomes closer to the display case, it will "sandwich" the jet, which causes a reduction in the mixing length, therefore resulting in a more "stable" jet. So, it is quite possible that jets that possess lower velocities may break down earlier and spread the cold air over a wider region due to a "weaker" vortex structure in front of them. It can also be seen that temperature outside the display case is colder than the surroundings due to the overspill. This temperature is about 60°F (15.6°C) in the immediate vicinity of the case, and increases to about 70°F (21.1°C) at about 2 ft (0.61 m) away from the middle of the case.

To develop confidence in the CFD prediction for the temperature field, the Refrigeration and Thermal Test Center at SCE performed an infrared imaging of the display case, and also closely monitored and maintained the DAV and DAT to establish a benchmarking set of data for CFD temperature profile validation. Figure 9 shows the infrared image of the display case with its corresponding temperature field. The infrared temperature readings were calibrated by nine thermocouples located on various locations on the surface of the flat plate, which is a black cardboard with emissivity of 0.96. This plate was located in the middle of air curtain. These thermocouples are traceable to the National Institute of Standards and Technology's standards.

A good comparison between the observed and measured data and its CFD counterpart in Fig. 8 can be observed. It can also be seen that the IR image has a lower resolution than the post-

program. In DPIV, the overall flowfield behavior is mapped by combining several frames. However, these frames may not be connected perfectly, i.e., there might be a gap, or slight overlap between frames. For these reasons, sometimes a sudden jump in the experimental results may be observed as the data is being extracted on a continuous line along the opening. A good agreement between the CFD model prediction and DPIV results can be observed.

It should be noted that we are performing a "global" comparison because the flowfield quantities such as the velocity components and turbulence intensity are not compared at a specific location. However, the end results, i.e., the infiltration rate and temperature field are of great practical importance, and conform part of the main focus of this paper. The comparison of the local velocity and turbulence intensity was performed, and will be the subject of another article. However, it should be mentioned that the rms (Root Mean Square) of the components of the velocity at the discharge grill is about 0.04 ms^{-1}, i.e., nearly 6% of the average velocity that reflects a turbulence intensity of 0.06. This
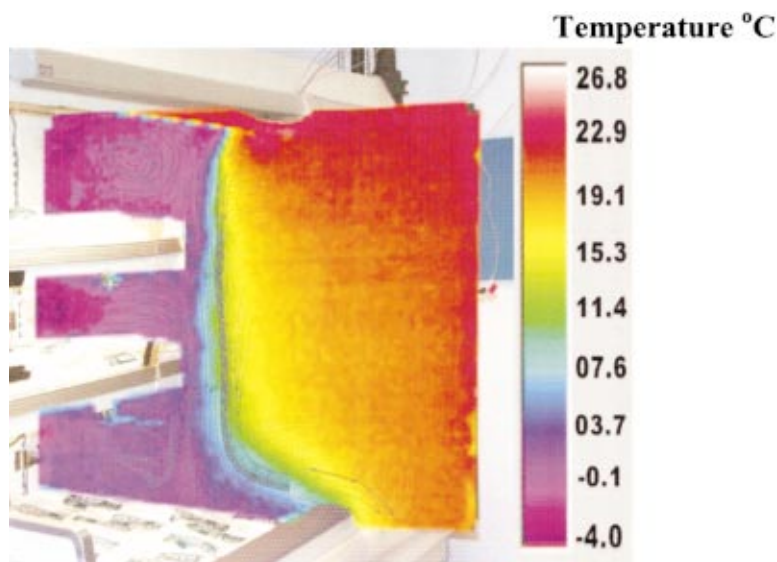

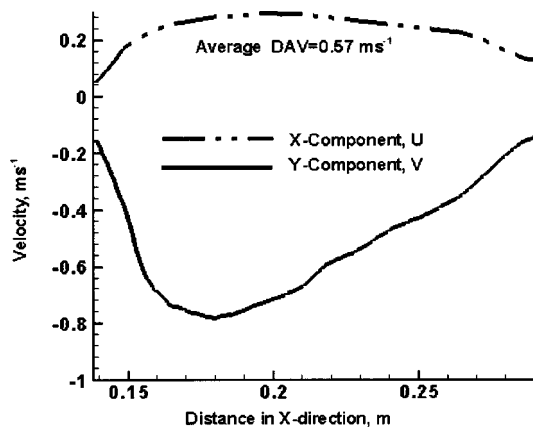**Fig. 9 Infrared image of the tested display case with corresponding temperature profile**

Table 2 Point data comparison for temperature in test scenario 1

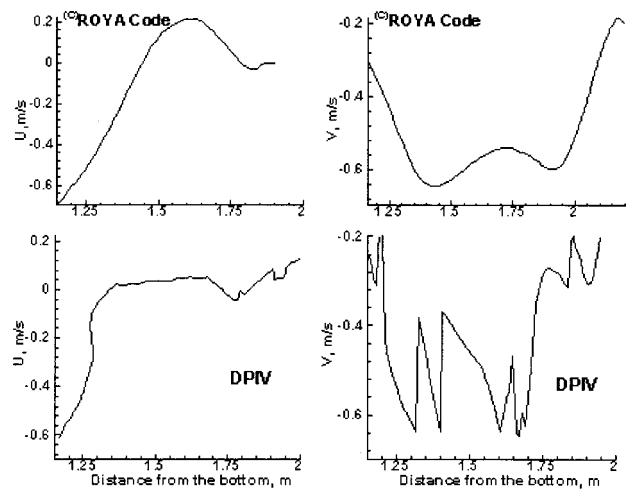| Location	RAT (°C)	ACT 1/3 (°C)	ACT 2/3 (°C)	Product temperature			
				Bottom front (°C)	Bottom rear (°C)	Top front (°C)	Top rear (°C)
Measured	5	7.7	5.5	3	−0.1	−1.6	−2.1
CFD	6	7.8	6	2.8	−0.5	−1.9	−2.2

processed CFD results. Furthermore, the field data comparison shows a good ''global'' agreement, i.e., they demonstrate that the air curtain is fairly effective in maintaining the temperature inside the display case over an acceptable range. The inside cold temperature gradually reaches the ambient air temperature due to the existing mixing region in front of the display case. It was mentioned earlier that in the computational model there is a supply of cold air distributed uniformly throughout the back panel. This has caused a slight shifting of the cold air curtain towards the outside of the case. The exact modeling of the perforated back panel is also possible, but time consuming. Since the effects of the temperature is fairly minor and most likely of the higher numerical order on the infiltration rate, no further refinements of the computational modeling of the back panel was performed. However, this global comparison is not sufficient and should be complemented by the point data comparison. To obtain such data, temperature sensors were placed at 1/3 and 2/3 distance of the opening from the discharge air grill or the air curtain temperature (ACT) (see Fig. 1), and at the front and back locations of the bottom and top

shelves. One sensor was also placed at the returned air grill location. The computational data can directly be extracted from the temperature contour plot by probing the field. The outcome of the measurements and computation is shown in Table 2.

The purpose of Test Scenario 2 is to demonstrate the dependency of the flowfield variables on the discharge air temperature. Therefore, the velocity of the air at the discharge grill is kept the same as Test Scenario 1, while its average temperature is increased by slightly more than 2°F (0.81°C) as indicated in Table 1. The results of CFD and DPIV studies reveal that the flowfield structure and variables are almost identical to those of Test Scenario 1. The calculated infiltration rate showed about 0.1% and 0.8% decrease for DPIV and CFD results, respectively. How-

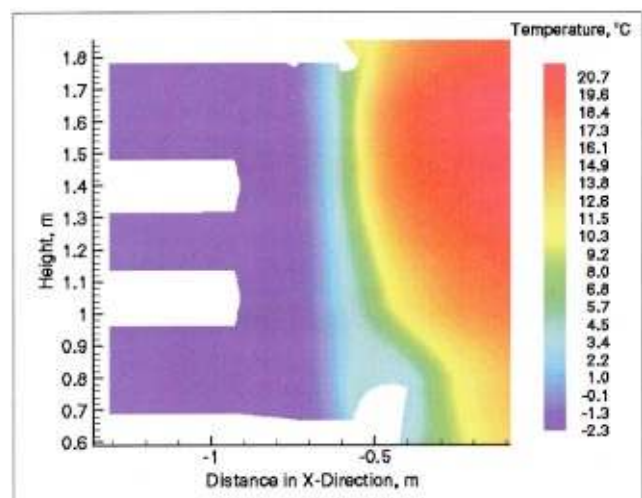Fig. 12 Components of velocity profile along the display case opening as predicted by the CFD and DPIV techniques for Test Scenario 3

Fig. 10 Velocity profile at the discharge grill for test Scenario 3 predicted by the DPIV technique
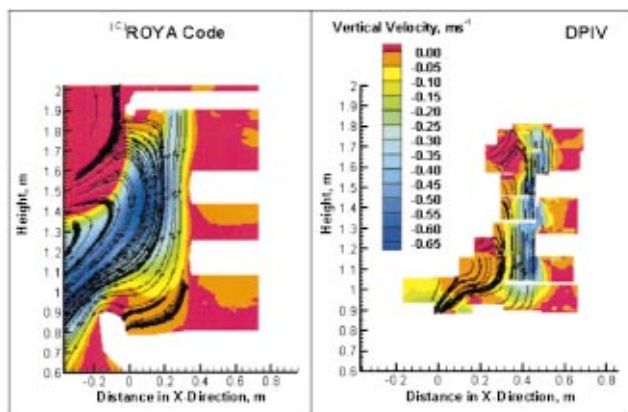
Fig. 11 Mean vertical velocity and streamline fields for test Scenario 3

Fig. 13 Temperature contours for test Scenario 3

Table 3 Volumetric flow rate of entrained air in CFM and m^3s^{-1}

Method	Test Scenario 1	Test Scenario 2	Test Scenario 3
DPIV	249.5(0.117751)	249.3(0.1176565)	218.8(0.1032621)
Entrained/Discharged	46.05%	46.56%	47.90%
CFD	251.8(0.118836)	249.9(0.1179397)	221.4(0.1044891)
Entrained/Discharged	47.02%	46.67%	48.47%

ever, no significant global change in the velocity profiles and streamline structure could be detected. Therefore, for the sake of brevity, no graphical display of streamlines and velocity contours is presented.

In Test Scenario 3, the inlet velocity of air at the discharge grill is lowered while the temperature is maintained the same as Test Scenario 1. Figure 10 shows the velocity profile at the discharge grill based on DPIV results. The same velocity profile was used as a boundary condition for the CFD analysis. The results of this Test Scenario 3 will lead to determining the dependency of the infiltration rate and temperature distribution on the momentum of the inlet air. It should also be added the reference coordinates for each test case is self-contained and not necessarily identical for each test case.

Figure 11 compares the vertical velocity contours and streamlines for the CFD and DPIV results. It seems that the flow structure and pattern resemble Test Scenario 1. However, the magnitude of the vertical velocity changes, therefore affecting the infiltration rate of the ambient air. The streamlines in the computational and experimental studies indicate that the inlet jet is still able to act as a curtain, traveling across the edge of the shelves, and downward onto the bottom shelf. The jet then turns to the left, and while some of the flow is brought back through a return grill, most of the jet is seen to be flowing over the edge of the display case to the outside. Though the inlet cold air velocity is smaller than Test Scenario 1, it is still able to entrain ambient air.

The quantitative comparison between the DPIV and CFD results for velocity components, similar to those in Test Scenario 1, is shown in Fig. 12. The velocity components show the same trend and magnitude for DPIV and CFD predictions, implying the accuracy of the CFD modeling.

Temperature contours for the Test Scenario 3 are shown in Fig. 13, and they basically indicate somewhat similar behavior as the Test Scenario 1. However, the colder temperature is further spread to the outside of the display case. This implies a less "stable" air curtain where a breakup of the flow is taking place before reaching to the bottom section. Furthermore, the air curtain spreads over a wider region after the onset of instability and causes a broader cold air band toward the bottom of the display case.

The volumetric flow rate of the entrained air into the display case is calculated for each of the above test scenarios using DPIV and CFD techniques independently. The entrained quantities are shown in Table 3. Computational and experimental methods yielded close results. Both approaches indicated that the entrainment rate is more sensitive to the magnitude of the DAV than the DAT. Furthermore, more than 40% of the total mass involved in the cooling is always "fresh and warm" ambient air that will significantly increase the cooling load.

Extension of Results

Reconciliation of the computational results with DPIV techniques developed a high degree of confidence in the CFD modeling approach used in this project. Based on the CFD methods used in this project, a parametric study has been performed to obtain the dependency of the infiltration rate of the ambient air on a wider range of the average velocity and temperature of the discharged air for the same geometrical configurations. For this purpose, the average discharged air velocity is varied from 90 to 180 ft-min^{-1} (0.4579 to 0.9144 ms^{-1}), and the average tempera-

ture ranges from 15 to 70°F (-9.45 to 21.12°C). In actual applications, however, open vertical, medium temperature display cases typically operate at much higher discharge air velocities than 90 ft-min^{-1} (0.4579 ms^{-1}).

The results of CFD simulation are graphically depicted in Fig. 14. The simulation results are curve fitted with a parabola, and again signifies the fact that the infiltration rate is a very weak function of the discharge air grill temperature and is mostly momentum driven. Furthermore, it can be seen that a decrease in the discharge air temperature will slightly increase the infiltration rate. The values in Table 3 can also be identified on this figure. However, it can be seen that the given parabola is very close to a line, and for simplicity and practical engineering problems a linear curve fit may be sufficient. Figure 15 shows a linear curve fit of
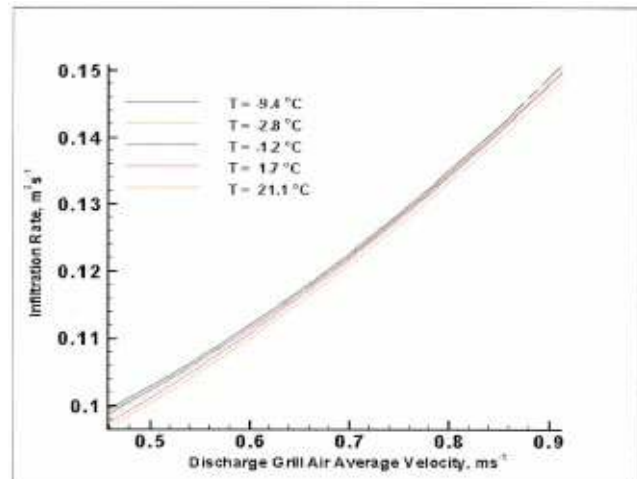
Fig. 14 Infiltration rate as a function of the discharge air average velocity and temperature by parabolic curve fit
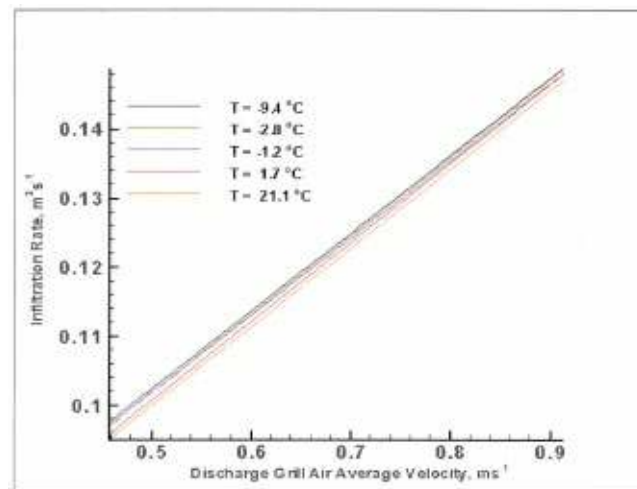
Fig. 15 Infiltration rate as a function of the discharge air average velocity and temperature by linear curve fit

the CFD simulation results, and they are very close to the results presented in Fig. 14. It can also be concluded that in cases where a high level of accuracy is not required, the temperature dependency of the infiltration rate might be thoroughly eliminated, and all curves or lines be collapsed into a single parabolic or linear curve. The maximum possible error in eliminating the temperature dependency can be calculated from either Fig. 14 or 15 to be about 2.5%. This can be evaluated from the volumetric flow rate difference between the minimum and maximum temperatures. The results of this parametric study provide information on the infiltration rate as a function of the discharge air velocity (DAV), and can be widely utilized by engineers to evaluate the cooling load and energy requirements for this particular display case. It is evident that the extension of these results to different display cases will provide valuable information to engineers, and will cut down the time consumed to evaluate cooling load calculations.

Conclusion

The combined computational and experimental study performed in this project demonstrates that calibrated CFD modeling can be used as a reliable and feasible tool for prediction of infiltration quantities in an open vertical display case. The project focused on examining the effects of DAV and DAT variation on the entrainment of air across the air curtain of one particular display case. Based on this approach, it was found that entrainment of air across the air curtain is predominantly momentum driven. Based on the results of this project, and without investigating the effects of other factors such as discharge air grill width or number of air bands, it can be concluded that changes that lead to better performance of the air curtain must primarily affect the momentum of the flowfield. This conclusion sets forth some of the options that are available for optimization of the air curtain design, such as the velocity distribution and its magnitude at the discharge grill. This paper also demonstrates that calibration of a CFD model with reliable and comprehensive experimental data is a prerequisite for generating reasonable and acceptable results. The marriage of the CFD simulation tool with powerful DPIV techniques can serve as an effective approach in design optimization of display case air curtains.

Nomenclature

ACT = Air Curtain Temperature
 (1/3 X: at 1/3 of the opening distance from the top)
 (2/3 X: at 2/3 of the opening distance from the top)
CFD = Computational Fluid Dynamics
CFM = Cubic Feet per Minute
DAT = Discharge Air Temperature
DAV = Discharge Air Velocity
DPIV = Digital Particle Image Velocimetry
LDV = Laser Doppler Velocimetry
NASA = National Aeronautics and Space Administration
NS = Navier-Stokes
RAT = Returned Air Temperature
RTTC = Refrigeration and Thermal Test Center

References

[1] Faramarzi, R., 1999, "Efficient Display Case Refrigeration," ASHRAE J., Nov., pp. 46–51.
[2] Stribling, D., Tassou, S. A., and Mariott, D., 1999, "A Two-Dimensional CFD Model of a Refrigerated Display Case," ASHRAE Trans., Nov., pp. 88–94.
[3] Navaz, H. K., 2000, ROYA©: A 2-D/3-D Code for Compressible, Incompressible Flows and Heat Transfer in Solids, Users Manual.
[4] Willert, C. E., and Gharib, M., 1991, "Digital Particle Image Velocimetry," Exp. Fluids, **10**, pp. 181–193.
[5] Westerweel, J., Dabiri, D., and Gharib, M., 1997, "The Effect of a Discrete Window Offset on the Accuracy of Cross-Correlation Analysis of PIV Recordings," Exp. Fluids, **23**, pp. 20–28.
[6] Gharib, M., and Dabiri, D., 1999, *An Overview of Digital Particle Image Velocimetry in Flow Visualization: Techniques and Examples*, Smiths, A. and Lim, T. T., eds.
[7] Navaz, H. K., and Dang, A. D., 1994, "The Development of the Liquid Thrust Chamber Performance (LTCP) Code for Turbulent Two-Phase Flow Combustion of Dense Sprays," Final Report Prepared for NASA/MSFC, Contract No. NAS8-38798.
[8] Navaz, H. K., and Berg, R. M., 1999, "Formulation of Navier-Stokes Equations for Moving Grid and Boundary," J. Propul. Power, **15**(1), Jan.–Feb.
[9] Navaz, H. K., and Berg, R. M., 1998, "Numerical Treatment of Multi-Phase Flow Equations with Chemistry and Stiff Source Terms," J. of Aerospace Science and Technology, **2**(3), Mar.–Apr., pp. 219–229.
[10] Dang, A. L., Navaz, H. K., and Coats, D. E., 1988, "PNS Solution of Non-Equilibrium Reacting Flow In Rocket Nozzles," 25th JANNAF Combustion Meeting, NASA/MSFC, Huntsville, AL.
[11] Berker, D. R., Coats, D. E., Dang, A. L., Dunn, S. S., and Navaz, H. K., 1990, "Viscous Interaction Performance Evaluation Routine for Nozzle Flows with Finite Rate Chemistry, (VIPER)," Final Report (Phase III) and Computer Users' Manual, Prepared for the Air Force Astronautics Laboratory, Edwards Air Force Base, California, Report No. AL-TR-90-042.